Semiclassical theory for the interaction dynamics of laser light and sodium atoms including the hyperfine structure

S. Dangel and R. Holzner
Physik-Institut der Universität Zürich, Winterthurerstrasse 190, CH-8057 Zürich, Switzerland
(Received 25 April 1997)

The conventional $J=1/2 \leftrightarrow J=1/2$ model is successful for the qualitative description of the interaction of sodium atoms and laser light tuned close to the atomic D_1 transition. However, time constants for dynamic effects due to optical pumping predicted by the model are about an order of magnitude too short compared to experimental observations. The inclusion of hyperfine states in the quantum-mechanical description of the atom leads to a satisfactory model that also predicts the correct absorption due to atomic diffusion and allows for the description of effects related to population trapping. This hyperfine model is derived in detail and compared with the $J=1/2 \leftrightarrow J=1/2$ approximation. [S1050-2947(97)00911-6]

PACS number(s): 32.80.Bx, 32.10.Fn, 03.65.Sq, 42.25.Bs

I. INTRODUCTION

In addition to a variety of other fascinating effects, the interaction of resonant laser light with alkali-metal atoms can create spatiotemporal intensity and polarization patterns in the propagating radiation field. For their theoretical description, a number of models have been developed that vary in complexity according to their aims. They have been optimized with regard to simplicity, treatability with analytical tools, inclusion of magnetic field effects, inclusion of the polarization properties of light, or the extension to other effects such as optical pumping, radiation trapping, or population trapping.

Probably the first and simplest model to describe atom-light interactions is the oscillating dipole model. By assuming an electron in the Coulomb potential of a positive charge driven by the oscillating electric field of a light wave, this entirely classical model is capable of describing absorption and dispersion effects that are coupled by the Kramers-Kronig relation and are expressed by the imaginary and real parts of a complex refractive index. The linewidth of the atomic transition, an intrinsic quantum-mechanical quantity, is interpreted as the damping of the oscillation and the binding potential determines the resonance oscillation frequency. From this model one can extract Beer's law for linear absorption in the weak signal approximation. It fails, however, for stronger radiation fields since in a real atom saturation occurs.

Saturation is taken into account by the optical Bloch equations [1], which represent the simplest semiclassical model where the light is a classical scalar wave and the atom is treated as a two-state quantum-mechanical system using a 2×2 density matrix. Since this treatment is nonperturbative (the terms of all orders in the electric field are retained), this model remains correct even for large-field amplitudes. A comparison [2] between the full QED treatment of the atom-radiation interaction [3] with the semiclassical approximation shows that the latter is a good approximation as long as the natural decay rate and the Rabi frequency are small compared to the optical transition frequency.

If effects due to the polarization of the electromagnetic radiation are to be described, the model for the atom must discriminate between the different angular momenta of the atomic states. A straightforward approach consists of rate equations [4] describing the mutual interaction of the atomic state populations and the radiation-field components. However, they do not contain coherences and are therefore not capable of describing diffraction that is essential for three-dimensional beam propagation. These effects require a semiclassical description employing the three-dimensional wave equation in combination with a quantum-mechanically derived atomic polarization term. In the case of the sodium D_1 transition, on which we shall concentrate in the following, a two-level four-state semiclassical model known as the $J=1/2 \leftrightarrow J=1/2$ model (or $J_{1/2}$ model) is adequate for the explanation of most effects. A general treatment of such a model has been given by Ducloy [5] based on irreducible tensors [6,7]. The model has been further developed for our specific experimental conditions by McCord and Ballagh in 1990 [8], however, only for the steady-state case. A one-pass system (not containing a cavity, a backreflecting mirror, or counterpropagating beams) is assumed. An arbitrary intensity and polarization pattern can be taken as input and its propagation through sodium vapor is then calculated numerically. The model includes diffraction, saturation, and optical-pumping-induced polarization effects. As shown in Fig. 1 (top), optical pumping [9] by circularly polarized light rearranges the initially equal populations of both ground states in such a way that the medium becomes transparent to the laser beam and all atoms populate the nonabsorbing ground state. Optical pumping represents a highly nonlinear mechanism even at very low light intensities. It leads to an intensity-dependent refractive index that is responsible for a variety of effects.

Some of these effects that we have experimentally observed are briefly summarized here for further reference. The simplest case of dynamic behavior, in which only a single circularly polarized beam ''pumps'' its way through the medium, is an important test case for the theory [4]. More complex effects are observed if two beams of different polarization are involved. Beam switching [4] occurs when a circularly polarized laser beam has optically pumped the me-

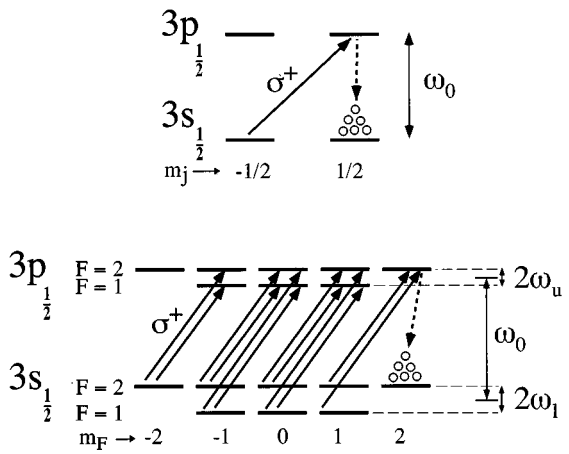

FIG. 1. Schematic representation of the sodium D_1 atomic transition. Top: neglecting the hyperfine structure leaves only four states ($J=1/2\leftrightarrow J=1/2$ model). Optical pumping, by, e.g., σ^+ circularly polarized light can occur directly between the $m_j=-1/2$ and $m_j=+1/2$ ground states. Bottom: full model with all hyperfine levels. Optical pumping occurs in several steps and is about an order of magnitude slower than in the $J=1/2\leftrightarrow J=1/2$ model. Relaxations other than the one to the pumped state are not shown.

dium and then a second beam of opposite circular polarization is switched on. As a result, the total transmitted light through the medium drops to zero since the mutual optical pumping of both beams redistributes the atoms in both ground states in a such way that both beams are absorbed completely. Another effect is beam bouncing [10], which occurs when two laser beams of opposite circular polarization are guided through sodium vapor with their geometrical intersection point in the middle of the cell and making an angle of about 5 mrad. The beams then deflect each other due to changes in the optical-pumping-induced refractive index that cause total internal reflection at the interface area close to the intersection point. A third effect is beam splitting [11], where two initially superimposed copropagating laser beams of opposite circular polarization suddenly split into two separated beams after having propagated a considerable distance through the medium. Also the effect of externally applied magnetic fields can be described by the model. Related experimental observations are the large-frequency shift of the absorption profile of circularly polarized light [12] and the deflection of a circularly polarized laser beam by the inhomogeneous transverse magnetic field of a current carrying wire [13,14].

Although the $J_{1/2}$ model describes most of the observed behavior qualitatively, it often fails to reproduce the true experimentally measured parameter values. It clearly fails, e.g., to account for a realistic description of the dynamics of optical-pumping-related phenomena. In the model the time scale of optical pumping is about one order of magnitude too fast compared to experimental observations [15]. Furthermore, the decay rate of the ground-state magnetization due to diffusion has to be adjusted for good agreement between experiment and theory with regard to the laser-beam absorption. Also in the case of external magnetic fields one has to vary the g factor of the lower level between $\frac{1}{2}$ and 2, depending on the observed effects, to match experimental results. All these shortcomings can be eliminated by the inclusion of the sodium hyperfine structure in the model. The importance of hyperfine effects has been mentioned previously, especially concerning population trapping [16–18] and optical-pumping time [15]. Due to the nuclear spin $I=3/2$ of sodium, 16 states have to be considered, 8 for the $3S_{1/2}$ and 8 for the $3P_{1/2}$ energy level. Even a simple rate equation model including the hyperfine states provides the correct optical-pumping time and light absorption [4]. However, as in the case of the $J=1/2\leftrightarrow J=1/2$ approximation, a semiclassical treatment is needed for the description of coherences and three-dimensional effects. The main part of the present paper is dedicated to the derivation of such a semiclassical hyperfine (HF) model and to the detailed explanation of the improvements compared to the semiclassical $J_{1/2}$ model.

Some aspects of the HF model can be understood intuitively. Due to the increased number of states [Fig. 1 (bottom)] one can see why the optical pumping process requires a longer time since an atom in the $m_F=-2$ ground state needs more pump cycles (''indirect'' pumping) until it reaches the only pumped state ($m_F=2$). One can also imagine that the unpolarized atoms that diffuse into the beam-interaction region contribute more strongly to the ground-state magnetization decay rate than in the $J_{1/2}$ model, in which half of the in-drifting atoms are already in the pumped state compared to only 1/8 in the case of the HF model. In addition to the improvements with respect to the $J_{1/2}$ model, the HF model also allows one to address fundamentally different questions. Population trapping, e.g., is shown to occur if the energy splitting of the hyperfine levels is decreased. The HF model also allows for different relaxation and dephasing rates for each rank (0–4) in the irreducible tensor representation, giving a total of 14 relaxation constants compared to only 3 in the $J_{1/2}$ model. The possible adaptation of the HF model to other atomic transitions and other alkali-metal atoms, as well as the case of a two-dimensional gas, is discussed in Sec. V B.

II. DERIVATION OF THE EQUATIONS

A. Assumptions

The atoms are considered to be at rest, which excludes the description of behavior caused by the Doppler effect or by velocity changing collisions. The motion of atoms is mimicked by adding appropriate relaxation terms into the density-matrix equations. The diffusion of atoms out of the laser beam area, e.g., is approximated by an exponential decay of the ground-state magnetization. In our experiments the use of argon as buffer gas reduces the diffusion rate of sodium atoms drastically. This approximates motionless atoms, inhibits nonlocal effects, and increases the transient time of atoms in the laser beam. The related low value for the ground-state magnetization decay rate is essential for efficient optical pumping in the relatively low-power beam. A further consequence of buffer gas is the homogeneous broadening of the atomic transition due to collisions. In the $J_{1/2}$ model this is the main reason to neglect hyperfine effects and Doppler broadening. In our HF model we still assume homogeneous broadening to be much larger than Doppler broadening, which can therefore be ignored.

The emitted radiation after a spontaneous decay of the excited atomic state is not taken into account and is considered to be lost to the system. This excludes radiation trapping effects and is usually a good approximation for low atomic densities and low light powers. Furthermore, the mutual interaction of atoms is neglected.

The laser linewidth is assumed to be zero, which is a good approximation for the experimental value of 1 MHz. Finally, although quadrupole and higher moments appear among the density-matrix elements, the wave equation in the dipole approximation will be used since the spatial variation of the field envelope $\vec{E}_0$ is assumed to be zero inside a volume element of atoms described by the density matrix.

B. Classical field equations

The laser light traveling along the z axis, defined as the quantization axis, is represented by the classical electric field

$$\vec{E}(\vec{r},t)=\mathrm{Re}[\vec{E}_0(\vec{r},t)e^{-i(\omega t-kz)}] = \tfrac{1}{2}[\vec{E}_0(\vec{r},t)e^{-i(\omega t-kz)}+\mathrm{c.c.}], \quad (1)$$

which is the product of the generally complex envelope $\vec{E}_0(\vec{r},t)$ of the field and the rapidly oscillating exponential function. Similarly, we write

$$\vec{P}(\vec{r},t)=\mathrm{Re}[\vec{P}_0(\vec{r},t)e^{-i(\omega t-kz)}] = \tfrac{1}{2}[\vec{P}_0(\vec{r},t)e^{-i(\omega t-kz)}+\mathrm{c.c.}] \quad (2)$$

for the electric polarization $\vec{P}$ due to the atom-light interaction. From the definition (1) follows the relation between the light intensity I (averaged over a period) and the envelope $\vec{E}_0$ given by

$$I=\frac{1}{2}\varepsilon_0 c|\vec{E}_0|^2. \quad (3)$$

Note that our definition of $\vec{E}_0$ is a factor of 2 larger than that in [5].

Inserting $\vec{E}$ and $\vec{P}$ into the classical wave equation derived from Maxwell's equations

$$\nabla^2\vec{E}-\frac{1}{c^2}\frac{\partial^2\vec{E}}{\partial t^2}=\frac{1}{\varepsilon_0 c^2}\frac{\partial^2\vec{P}}{\partial t^2}, \quad (4)$$

we obtain

$$\nabla^2\vec{E}_0+2ik\frac{\partial\vec{E}_0}{\partial z}+\frac{2i\omega}{c^2}\frac{\partial\vec{E}_0}{\partial t}-\frac{1}{c^2}\frac{\partial^2\vec{E}_0}{\partial t^2} = -\frac{k^2}{\varepsilon_0}\vec{P}_0-\frac{2i\omega}{\varepsilon_0 c^2}\frac{\partial\vec{P}_0}{\partial t}+\frac{1}{\varepsilon_0 c^2}\frac{\partial^2\vec{P}_0}{\partial t^2} \quad (5)$$

for the relation between the envelopes $\vec{E}_0$ and $\vec{P}_0$. Within the slowly varying envelope approximation, the higher derivatives of $\vec{E}_0$ and $\vec{P}_0$ are neglected, which leads to the final equation

$$\left[\left(\frac{\partial}{\partial z}+\frac{1}{c}\frac{\partial}{\partial t}\right)-\frac{ic}{2\omega}\left(\frac{\partial^2}{\partial x^2}+\frac{\partial^2}{\partial y^2}\right)\right]\vec{E}_0(\vec{r},t)=\frac{i\omega}{2c\epsilon_0}\vec{P}_0(\vec{r},t). \quad (6)$$

The approximation is justified by the large value of ω. In addition to restricting the light propagation to the positive z direction, it also allows for larger time steps in the numerical solution of the wave equation (reduced stiffness) [19].

We express $\vec{E}_0$ and $\vec{P}_0$ in the standard spherical representation with the base vectors $\vec{e}_q$,

$$\vec{e}_{\pm1}=\mp\sqrt{\tfrac{1}{2}}(\vec{e}_x\pm i\vec{e}_y), \quad \vec{e}_0=\vec{e}_z, \quad (7)$$

as

$$\vec{E}_0=-E_0^-\vec{e}_+-E_0^+\vec{e}_-,$$
$$\vec{P}_0=-P_0^-\vec{e}_+-P_0^+\vec{e}_-, \quad (8)$$

with $E_0^\pm$ and $P_0^\pm$ denoting the right- and left-hand circularly polarized components of $\vec{E}_0$ and $\vec{P}_0$, respectively. No z components occur since the laser beam is restricted to propagate along the z axis.

C. Quantum-mechanical atomic equations

The macroscopic polarization $\vec{P}$ is essentially the expectation value of the dipole operator obtained from the density operator ρ, which obeys the modified von Neumann equation

$$\frac{\partial\rho}{\partial t}=-\frac{i}{\hbar}[H,\rho]+\left(\frac{\partial\rho}{\partial t}\right)_{\mathrm{relax}}, \quad (9)$$

where the Hamiltonian H is

$$H=H_0+H_{\mathrm{laser}}+H_{\mathrm{magnet}}. \quad (10)$$

Equation (9) is, in our case of 16 possible atomic states, an equation between 16×16 matrices, yielding 256 coupled ordinary differential equations for the matrix elements of ρ. Normally one develops ρ in the standard (energy) basis $|\alpha,F,m\rangle$, where F is the total angular momentum, m its projection on the z axis, and α the other indices necessary to specify the state. In our case, $\alpha=l$ denotes the lower state $3s_{1/2}$ and $\alpha=u$ the upper state $3p_{1/2}$. Due to the symmetry of the problem, however, it is useful to develop the density matrix onto a basis of irreducible tensors [6] defined as

$${}^{FG}_{\alpha\beta}T^k_q=\sum_{m,n}(-1)^{G-n}\langle F,G,m,-n|k,q\rangle|\alpha,F,m\rangle\langle\beta,G,n|, \quad (11)$$

which is a linear transformation of the standard basis. $\langle F,G,m,-n|k,q\rangle$ is the Clebsch-Gordan coefficient coupling the angular states F,m and $G,-n$ to the state k,q. The operators ${}^{FG}_{\alpha\beta}T^k_q$ can be seen as a generalization of the Pauli spin matrices for a spin-1/2 system. The density operator ρ is then expanded on this basis introducing the time-dependent coefficients ${}^{FG}_{\alpha\beta}\rho^k_q(t)$ as

$$\rho(t)=\sum_{\alpha,\beta,F,G,k,q} {}^{FG}_{\alpha\beta}\rho^k_q(t)\,{}^{FG}_{\alpha\beta}T^k_q. \tag{12}$$

In addition to irreducibility with regard to rotations, this expansion of ρ gives access to the results of irreducible set theory and allows for a comparison with results from other authors since it adheres to the standard normalization and phase conventions. Also, in contrast to the standard components, the irreducible components of ρ generally have a deeper physical meaning since they represent quantities such as population, orientation, and alignment, according to their rank k.

The expectation value of any operator A is

$$\langle A\rangle=\mathrm{Tr}(\rho A) \tag{13}$$

and the expectation values of the irreducible tensor operators T are

$$\langle {}^{FG}_{\alpha\beta}T^k_q\rangle={}^{FG}_{\alpha\beta}\rho^k_q{}^*. \tag{14}$$

It is therefore straightforward to find the expectation value of $\vec{P}_0$ used in the wave equation (5) once we have expressed the dipole operator in terms of the irreducible tensors. Other useful relations are the matrix element of the tensor T in the standard basis

$$\langle \alpha,F',m'|{}^{F'F}_{\alpha\beta}T^k_q|\beta,F,m\rangle = (-1)^{F'-m'}\sqrt{2k+1}\begin{pmatrix} F' & k & F\\ -m' & q & m\end{pmatrix}, \tag{15}$$

the Hermiticity relation between matrix elements

$${}^{FG}_{\alpha\beta}\rho^k_q=(-1)^{F-G-q}\quad {}^{GF}_{\beta\alpha}\rho^k_{-q}{}^*, \tag{16}$$

and the population conservation relation $\mathrm{Tr}\rho=1$, which in our case gives

$$\sqrt{3}({}^{11}_{ll}\rho^0_0+{}^{11}_{uu}\rho^0_0)+\sqrt{5}({}^{22}_{ll}\rho^0_0+{}^{22}_{uu}\rho^0_0)=1. \tag{17}$$

The first component of H, the Hamiltonian of the unperturbed atom, is

$$H_0=\sum_{\alpha=l,u}\sum_F E_{\alpha,F}\sqrt{2F+1}\,{}^{FF}_{\alpha\alpha}T^0_0, \tag{18}$$

where $E_{\alpha,F}$ is the energy of level α with total angular momentum F. As indicated in Fig. 1, we define the D_1 transition frequency ω_0 as

$$\hbar\omega_0=\frac{E_{u,1}+E_{u,2}}{2}-\frac{E_{l,1}+E_{l,2}}{2} \tag{19}$$

and the hyperfine splitting energies as

$$\Delta E_{HF,l}=2\hbar\omega_l=E_{l,2}-E_{l,1},$$
$$\Delta E_{HF,u}=2\hbar\omega_u=E_{u,2}-E_{u,1}. \tag{20}$$

The laser-atom detuning is defined as

$$\Delta\omega=\omega-\omega_0. \tag{21}$$

Note that in the case of line broadening, in contrast to the $J_{1/2}$ model, the frequency of maximum absorption is not at zero detuning for the HF model. For typical parameter values in the present paper, the absorption maximum is shifted about 0.5 GHz towards the low-frequency side.

D. Interaction with the laser beam

The Hamiltonian of the atom-light interaction is

$$H_{\mathrm{laser}}=-\vec{E}\cdot\vec{\mathsf{D}}, \tag{22}$$

where $\vec{\mathsf{D}}$ is the dipole operator. If we express the electric field (1) and the dipole operator in standard spherical components (7), we obtain

$$\vec{E}\cdot\vec{\mathsf{D}}=-\tfrac{1}{2}(E_0^-e^{-i\omega t}-E_0^+{}^*e^{+i\omega t})\mathsf{D}^+ -\tfrac{1}{2}(E_0^+e^{-i\omega t}-E_0^-{}^*e^{+i\omega t})\mathsf{D}^-. \tag{23}$$

The dipole operator is a tensor of rank 1 and therefore its matrix elements are (compare [20], Eq. 5.4.1)

$$\langle F',m',J',I|\mathsf{D}_q|F,m,J,I\rangle = (-1)^{F'-m'}\begin{pmatrix} F' & 1 & F\\ -m' & q & m\end{pmatrix}\langle F',J',I||\mathsf{D}||F,J,I\rangle. \tag{24}$$

Since $\vec{\mathsf{D}}$ only operates on the first part ($\vec{J}$) of the coupled angular momenta $\vec{F}=\vec{J}+\vec{I}$ ([20], Eq. 7.1.7), the reduced matrix element on the right-hand side is

$$\langle F',J',I||\mathsf{D}||F,J,I\rangle=(-1)^{J'+I+F+1}\sqrt{(2F+1)(2F'+1)}\times\begin{Bmatrix} J' & F' & I\\ F & J & 1\end{Bmatrix}\langle J'||\mathsf{D}||J\rangle, \tag{25}$$

while the final reduced matrix element is an integral over the radial wave functions R_l given by

$$\langle J'||\mathsf{D}||J\rangle=\sqrt{\frac{2}{3}}\int_0^\infty R_{l=1}R_{l=0}r^3dr\equiv\sqrt{\frac{2}{3}}d. \tag{26}$$

The integral cannot be evaluated directly, but is related to the natural decay rate γ_{nat} by [21]

$$d=3\sqrt{\frac{\gamma_{\mathrm{nat}}\pi\hbar c^3\varepsilon_0}{2\omega_0^3}}. \tag{27}$$

For the sodium D_1 transition, we have $I=\frac{3}{2}$, $J=J'=\frac{1}{2}$, and $F=1,2$. Summarizing the above relations together with Eq. (15) leads to

$$\mathsf{D}_q=\frac{d}{\sqrt{18}}[-{}^{11}_{lu}T^1_q-{}^{11}_{ul}T^1_q+\sqrt{5}({}^{21}_{lu}T^1_q-{}^{12}_{ul}T^1_q-{}^{12}_{lu}T^1_q+{}^{21}_{ul}T^1_q+{}^{22}_{lu}T^1_q+{}^{22}_{ul}T^1_q)]. \tag{28}$$

Only $\mathsf{D}_{\mp1}$ are needed since in our case the laser beam propagates along the z axis.

E. Magnetic field

The Hamiltonian of the magnetic-field interaction is

$$H_{\text{magnet}}=\frac{\mu_0 g_J}{\hbar}\vec{B}\cdot\vec{\mathsf{J}}+\frac{\mu_{\text{nuc}} g_I}{\hbar}\vec{B}\cdot\vec{\mathsf{I}} \tag{29}$$

as long as H_{magnet} is smaller than the hyperfine interaction (low-field approximation). The second term is three orders of magnitude smaller than the first due to the small nuclear magnetic moment. This alone is no reason to neglect it, since even small couplings between the equations for the density-matrix elements can have large effects. However, this term does not introduce couplings that were not already present in the first term and will therefore be neglected. Like the dipole operator D, the operator J is a tensor of rank 1, so the same treatment as before can be applied, except for the final reduced matrix element (see [20], 5.4.3)

$$\langle J'||\mathsf{J}||J\rangle=\delta_{JJ'}\hbar\,\delta_{\alpha\beta}\sqrt{J(J+1)(2J+1)}. \tag{30}$$

Again, using Eq. (15), we obtain

$$g_J\mathsf{J}_q=\frac{\hbar}{2\sqrt{2}}\sum_{\alpha=l,u} g_{J,\alpha}[-{}^{11}_{\alpha\alpha}T^1_q+\sqrt{5}(-{}^{12}_{\alpha\alpha}T^1_q+{}^{21}_{\alpha\alpha}T^1_q+{}^{22}_{\alpha\alpha}T^1_q)], \tag{31}$$

with $g_{J,l}=2$ and $g_{J,u}=\frac{2}{3}$. Note that the reduction of the g_J factors by $\pm(2I+1)$ used by many authors (e.g., [22]) is already included in this treatment.

F. Evaluation of $[H,\rho]$

We evaluate Eq. (9) *without* relaxation terms in H. Those terms are added directly into the equations later. H and ρ can be multiplied directly in the irreducible tensor basis using the relation

$$\begin{aligned}{}^{FG}_{\alpha\beta}T^k_q\,{}^{F'G'}_{\alpha'\beta'}T^{k'}_{q'}=&\sum_{k'',q''}(-1)^{G'+F+k'-k+k''-q''}\\&\times\delta_{GF'}[(2k+1)(2k'+1)(2k''+1)]^{1/2}\\&\times\begin{pmatrix}k&k'&k''\\q&q'&-q''\end{pmatrix}\begin{Bmatrix}k&k'&k''\\G'&F&F'\end{Bmatrix}{}^{FG'}_{\alpha\beta'}T^{k''}_{q''}.\end{aligned} \tag{32}$$

Comparing the coefficients of the corresponding tensors on the left- and right-hand sides of Eq. (9) leads to a system of 256 ordinary differential equations for the density-matrix elements. After the substitution

$$\begin{aligned}{}^{FG}_{lu}\rho^k_q&\rightarrow e^{+i\omega t}\,{}^{FG}_{lu}\tilde{\rho}^k_q,\\{}^{FG}_{ul}\rho^k_q&\rightarrow e^{-i\omega t}\,{}^{FG}_{ul}\tilde{\rho}^k_q,\end{aligned} \tag{33}$$

the terms oscillating at optical frequencies in the products ρH and $H\rho$ of Eq. (9) are assumed to average to zero (rotating-wave approximation [23]). For example, in

$$\cdots E_0^+ * e^{2i\omega t}-E_0^-\cdots \tag{34}$$

the $e^{2i\omega t}$ term is ignored. The rotating-wave approximation restricts the useful time domain to $t\gg 1/\omega$ due to averaging over the light oscillations.

G. Relaxations

A disadvantage of a semiclassical (non-QED) treatment of the light-matter interaction is that the various relaxation effects have to be added phenomenologically instead of being included in the Hamiltonian. We will now discuss the different relaxation expressions $(\dot{\rho})_{\text{relax}}$.

For our case with the coupling $\vec{F}=\vec{J}+\vec{I}$ (hyperfine structure small compared to the fine structure), the additional terms in the density-matrix equations due to natural decay are [24]

$$({}^{FG}_{ll}\dot{\rho}^k_q)_{\text{nat relax}}=\sum_{F',G'}{}^{F'G'}_{FG}\zeta^k\quad{}^{F'G'}_{uu}\rho^k_q, \tag{35}$$

with

$$\begin{aligned}{}^{F'G'}_{FG}\zeta^k=&(-1)^{F+F'+k+1}\gamma_{\text{nat}}(2J'+1)\\&\times\sqrt{(2F+1)(2G+1)(2F'+1)(2G'+1)}\\&\times\begin{Bmatrix}F&G&k\\G'&F'&1\end{Bmatrix}\begin{Bmatrix}G'&G&1\\J&J'&I\end{Bmatrix}\begin{Bmatrix}F'&F&1\\J&J'&I\end{Bmatrix}.\end{aligned} \tag{36}$$

The ll-matrix elements relax due to diffusion and collision processes. We will use

$$({}^{FG}_{ll}\dot{\rho}^k_q)_{\text{relax}}=({}^{FG}_{ll}\dot{\rho}^k_q)_{\text{nat relax}}-\gamma^k_{ll}\;{}^{FG}_{ll}\rho^k_q. \tag{37}$$

For all other (uu, lu, and ul) elements we add the terms

$$({}^{FG}_{\alpha\beta}\dot{\rho}^k_q)_{\text{relax}}=-\gamma^k_{\alpha\beta}\;{}^{FG}_{\alpha\beta}\rho^k_q, \tag{38}$$

where the γ^k_{uu} are the sum of the natural decay rate and collisional rates of the upper level, γ^k_{ll} the decay rates of the lower level mainly due to diffusion processes, and γ^k_{lu} the multipole dephasing rates. Hermiticity demands that $\gamma^k_{lu}=\gamma^k_{ul}$ and enforcing population conservation (17) results in $\gamma^0_{ll}=0$ and $\gamma^0_{uu}=\gamma_{\text{nat}}$, which excludes nonradiative decays.

As initial conditions, before laser light enters the sodium vapor cell, all density-matrix elements are zero except

$${}^{11}_{ll}\rho^0_0(t=0)=\frac{\sqrt{3}}{8},\quad{}^{22}_{ll}\rho^0_0(t=0)=\frac{\sqrt{5}}{8}. \tag{39}$$

These elements describe the population in the $F=1$ and $F=2$ ground states, respectively. Initially all atoms occupy one of these states. When the laser is turned off ($E_0^+=E_0^-=0$), the equation for the population of the lower $F=1$ level becomes

$${}^{11}_{ll}\dot{\rho}^0_0=\frac{\gamma_{\text{nat}}}{6}({}^{11}_{uu}\rho^0_0+\sqrt{15}\,{}^{22}_{uu}\rho^0_0). \tag{40}$$

TABLE I. Number of generally complex ordinary differential equations needed to calculate the electric polarization (43) for various $\vec{E}$ and $\vec{B}$ field configurations. In all cases the number can be further reduced by one using the population conservation relation (17).

Setup	Number of equations
$B_{\text{trans}} \neq 0$, $\vec{E}_0$ arbitrary	136
$E_0^+ \neq 0$, $E_0^- \neq 0$, $B_{\text{trans}} = 0$	72
$E_0^- = 0$, $B_{\text{trans}} = 0$	34

If the laser has been off for a long time, the upper-state populations ${}^{11}_{uu}\rho^0_0$ and ${}^{22}_{uu}\rho^0_0$ are zero. This means that ${}^{11}_{ll}\rho^0_0$ remains stationary and does not relax to the initial equilibrium population of $\sqrt{3}/8$ due to atomic diffusion in and out of the beam area. We simulate this by adding the following diffusion terms to the equations:

$$\begin{aligned}
({}^{11}_{ll}\dot{\rho}^0_0)_{\text{diff}} &= -\gamma_{\text{diff}}({}^{11}_{ll}\rho^0_0 - \sqrt{3}/8), \\
({}^{22}_{ll}\dot{\rho}^0_0)_{\text{diff}} &= -\gamma_{\text{diff}}({}^{22}_{ll}\rho^0_0 - \sqrt{5}/8), \\
({}^{11}_{uu}\dot{\rho}^0_0)_{\text{diff}} &= -\gamma_{\text{diff}}\,{}^{11}_{uu}\rho^0_0, \\
({}^{22}_{uu}\dot{\rho}^0_0)_{\text{diff}} &= -\gamma_{\text{diff}}\,{}^{22}_{uu}\rho^0_0 .
\end{aligned} \tag{41}$$

The additional decay rates for the upper level are negligible compared to the rates introduced in Eq. (38), but they are essential for conserving the total population.

H. Expectation value of $\vec{P}_0$

The mean value of the macroscopic polarization is

$$\vec{P}_0 = -n\langle D_{-1}\rangle \vec{e}_+ - n\langle D_{+1}\rangle \vec{e}_- , \tag{42}$$

where n is the volume density of atoms. Using Eq. (14) and the expression for the dipole operator (28) and comparing the result with Eq. (8), we obtain the mean value of the polarization envelope components

$$P_0^q = \frac{2nd}{\sqrt{18}}[{}^{11}_{lu}\tilde{\rho}^{\,1}_q + \sqrt{5}(-{}^{12}_{lu}\tilde{\rho}^{\,1}_q + {}^{21}_{lu}\tilde{\rho}^{\,1}_q + {}^{22}_{lu}\tilde{\rho}^{\,1}_q)]^* . \tag{43}$$

The size of the complex differential equation system for the density-matrix elements needed to evaluate Eq. (43) depends on the specific symmetry defined by the polarization components of the laser light and the components of the magnetic field. The hermiticity relation (16) reduces the number of equations from 256 to 136 for arbitrary light polarization and magnetic field (Table I). If no transverse magnetic field (B_{trans}) is applied, the number of equations is 72, even if a longitudinal magnetic field (B_z) is present. The longitudinal field does not change the symmetry of the setup and therefore does not introduce new transitions between atomic states involving additional density-matrix elements. For the case of only one circular polarization ($E_0^- = 0$) and no transverse magnetic field, the size of the system reduces even further to 34 equations, which are given in Appendix A. In all cases, the set of equations can be reduced by one if the population conservation relation (17) is applied. The equations for the 16 elements ${}^{FF}_{\alpha\alpha}\rho^k_0$ are real, while all others are generally complex.

I. Numerics

For given electric and magnetic fields, the time evolution of the density matrix can be numerically evaluated by using, e.g., a Runge-Kutta integration method. If light propagation has to be included, the density matrix equations have to be solved *locally*, coupled to the partial differential equations (6). We plan to give a detailed description of a fast algorithm solving these equations in time and three-dimensional space elsewhere [19].

Even though only the electric dipole is used in the wave equation (due to the approximation that the electric-field gradient is virtually zero over a sufficiently small volume of atoms), none of the elements of the density matrix, not even for $k \geqslant 3$, have been approximated by zero, as can be done for steady-state calculations [25]. We found that, especially for short-time simulations (within a few Rabi oscillations), such approximations would lead to large errors in the dynamic evolution compared to a full solution of all equations.

The numerical values used in the calculations are

$$\gamma_{\text{nat}} = 6.25\times 10^7 \ \text{s}^{-1}, \tag{44}$$

$$d = 2.6\times 10^{-29} \ \text{Cm}, \tag{45}$$

$$\Delta E_{HF,l} = \hbar \times 2\pi \times 1772 \ \text{MHz}, \tag{46}$$

$$\Delta E_{HF,u} = \hbar \times 2\pi \times 189 \ \text{MHz}. \tag{47}$$

The relaxation rates γ^k_{ll} and γ_{diff} have been estimated from the average diffusion time of Na atoms through the laser beam. They are typically of the order of $10^4\ \text{s}^{-1}$. The rates γ^k_{uu} contain the natural and collisional decay rates and are therefore equal to or larger than γ_{nat}. The model is not very sensitive to these rates, and for simplicity we set all of them equal to γ_{nat}. Finally, the rates γ^k_{lu} can be determined by the absorption width [26]. They are about $10^{10}\ \text{s}^{-1}$ for an argon buffer gas pressure of 240 Torr at 500 K.

By setting $\gamma^k_{\alpha\beta}$ to be equal for each rank k, we disregard possible differences between the relaxation rates for populations, orientations, alignments, etc. However, if such differences should become of importance in the future, they can be added to the equations in a straightforward manner. This would be difficult if ρ had been expanded in the standard basis.

III. COMPARISON WITH THE $J=1/2 \leftrightarrow J=1/2$ MODEL

The semiclassical $J_{1/2}$ model that we compare with the HF model is a special case of the equations in [5]. It has been published in more detail in [8], however, for the steady state only. For completeness, the corresponding *time-dependent* density-matrix equations are given in Appendix B.

The main difference between the $J_{1/2}$ and HF model concerning optical pumping is the increased number of atomic states in the latter. The ''indirect'' optical pumping in the HF model is about an order of magnitude slower than in the $J_{1/2}$

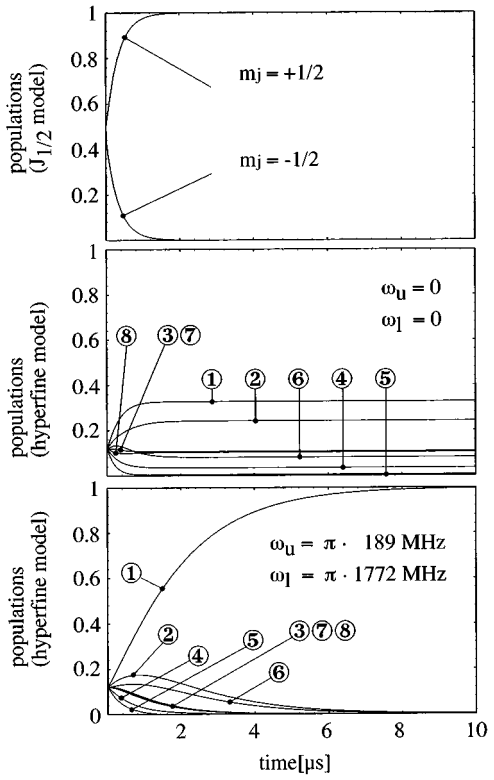

FIG. 2. Evolution of the lower-level populations when a circularly polarized light source with zero detuning ($\omega=\omega_0$) is turned on at $t=0$. The lower-level relaxation constants γ_{ll}^k and $\gamma_{\rm diff}$ have been set to zero. The electric field is $E_0^+=3000$ V/m, corresponding to an intensity of 11 900 W/m^2. Top: fast and complete optical pumping in the $J=1/2\leftrightarrow J=1/2$ model. Center: fast and incomplete optical pumping due to population trapping when the hyperfine energy splittings are neglected in the HF model. Bottom: slow and complete optical pumping with the correct hyperfine energies. The hyperfine states are indicated by 1: $F=2$, $m_F=+2$; 2: $F=2$, $m_F=+1$; 3: $F=2$, $m_F=0$; 4: $F=2$, $m_F=-1$; 5: $F=2$, $m_F=-2$; 6: $F=1$, $m_F=+1$; 7: $F=1$, $m_F=0$; 8: $F=1$, $m_F=-1$.

model since it involves several pump cycles between substates. A simple rate model [4] including hyperfine levels but no hyperfine energy splittings (and no coherences) confirmed this behavior. Since the absorption width due to buffer gas collisions is considerably larger than the hyperfine energy splittings, we expected that the hyperfine splitting energies would not be important also for the semiclassical HF model. However, for $\omega_l=\omega_u=0$ the optical pumping is incomplete and again too fast as shown in a simulation (Fig. 2, center) of the time evolution of the hyperfine density-matrix components under the influence of circularly polarized light. The reason is an effect known as ''population trapping'' [27,16–18], which cannot occur in the $J_{1/2}$ approximation or in the hyperfine rate equation model. Population trapping appears when two lower states, e.g., the two $m_F=-1$ states, are coupled to the same upper state (e.g., one of the $m_F=0$ states; see Fig. 1). The coherence between the two ground states then suppresses optical pumping. In the references mentioned above, two coherent laser fields are involved and the trapping effect is strongest when each one is exactly on resonance with one of the two transitions, even for

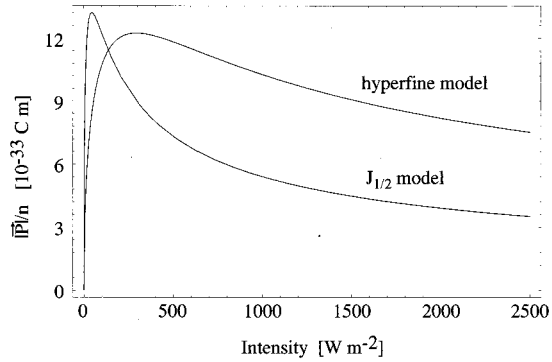

FIG. 3. Steady-state polarization per atom for circularly polarized light ($E_0^-=0$) as a function of the light intensity I with $\gamma_{ll}^k=\gamma_{\rm diff}=1.55\times10^4$ s^{-1} and $\omega=\omega_0$. For typical laser light intensities, the polarization (and therefore the absorption in our case) is always larger in the hyperfine model. This effect reverses for I below about 140 W/m^2.

$\omega_l,\omega_u>0$. In our case of only one laser field, the effect is strongest if the two atomic transition frequencies are equal and the laser is on resonance with both ($\omega_l=\omega_u=\Delta\omega=0$). As soon as the hyperfine energy splittings are nonzero ($\omega_l,\omega_u>0$), the coherences causing population trapping are reduced and complete optical pumping is possible (Fig. 2, bottom). The effect is directly reflected in the density matrix equations (Appendix A). For example, the term $-(2i\omega_l+\gamma_{ll}^1)\,{}_{ll}^{21}\rho_0^1$ in the equation for ${}_{ll}^{21}\dot\rho_0^1$ oscillates with ω_l and averages to zero with large enough hyperfine energy splitting. This is an example of very small terms in H having a large effect on the density-matrix evolution. In addition to the longer pumping time, another difference relative to the $J_{1/2}$ model is the considerably larger influence of the (diffusion dominated) relaxation rates γ_{ll}^k. The absorption of a circularly polarized laser beam is usually much larger in the HF model than in the $J_{1/2}$ approximation for the same relaxation rates. The comparison of the rate equation systems for both cases [4] leads to a simple explanation: In the $J_{1/2}$ model one-half of the atoms entering the laser beam through diffusion are already in the pumped state, while in the HF model this ratio is only 1/8, which leads to the larger absorption of the beam. However, this absorption difference is more complicated for the semiclassical models, as can be seen in Fig. 3. It depends not only on the values of γ_{ll}^k and $\gamma_{\rm diff}$, but also on the intensity of the beam. For typical values of the relaxation constants for sodium cells containing argon buffer gas, the absorption is larger in the HF model for intermediate and large light intensities, but smaller for intensities below a certain threshold, which depends on the values of γ_{ll}^k and $\gamma_{\rm diff}$. This unexpected behavior is the subject of further investigation.

A full three-dimensional and time-dependent simulation of both the $J_{1/2}$ and HF semiclassical model reveals the difference in absorption as well as in the optical pumping time (Fig. 4). Only the HF model describes the experiment correctly. In the experiment, the laser has been tuned to the frequency of maximum absorption. Due to the definition of ω_0, this corresponds to a detuning of $\omega-\omega_0=-2\pi\times0.5$ GHz in the HF model and to zero detuning in the $J_{1/2}$ model. The remaining differences between the HF model and the

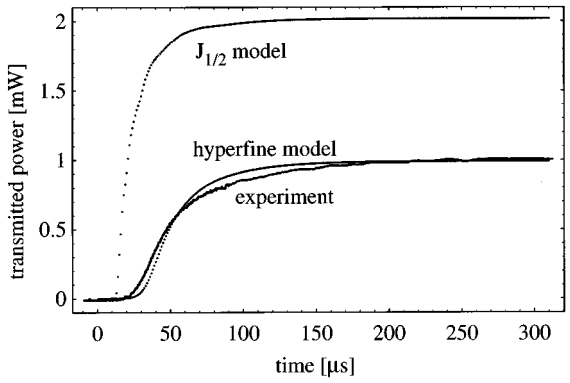

FIG. 4. Comparison of an experimental transient with the two theories. A Gaussian beam of 4 mW has been turned on at $t=0$ and the transmitted power behind a 6.5-cm-long sodium vapor cell ($T=200°$ C) is observed. Other parameters of the simulation are $\gamma_{ll}^{k}=\gamma_{\mathrm{diff}}=1.55\times10^{4}\ \mathrm{s}^{-1}$ and $\gamma_{lu}^{k}=1.0\times10^{10}\ \mathrm{s}^{-1}$. The parameters of the experiment have been directly inserted into the models for the numerical simulations. There are no fitting parameters, but the input and the output power have been corrected for cell window losses.

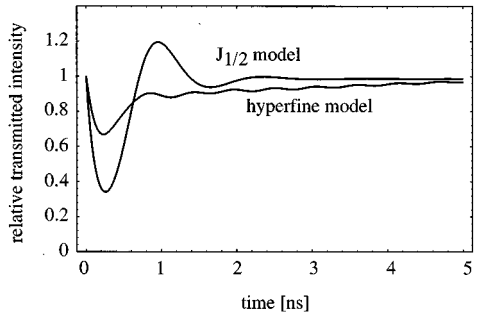

FIG. 5. Relative transmitted intensity behind 10^{-3} monolayers of sodium. The incoming beam is assumed to be a circularly polarized plane wave with $1.2\times10^{6}\ \mathrm{W/m^2}$ intensity, turned on at $t=0$. The hyperfine model predicts a reduced but longer oscillation.

experiment are due mainly to imperfect Gaussian beam profiles. Residual magnetic fields in the experiment are below 3 mG and have little influence, as was confirmed by numerical simulations.

A further difference between the models is the effect of an external magnetic field. The g_J factors $g_{J,l}=2$ and $g_{J,u}=\frac{2}{3}$ of the $J_{1/2}$ model are effectively reduced by a factor 4 for $F=2$ and -4 for $F=1$ in the HF model, equivalent to a ''distribution'' of the g_J factors over the magnetic hyperfine sublevels. The $J_{1/2}$ model contains only a single Larmor frequency for the ground state and its predicted value is four times larger than the experimental value of about 700 kHz/G. Also, the model fails to describe nuclear Zeeman effects, e.g., the different magnetic transition frequencies for the ground state [15]. However, due to the g_J-factor distribution mentioned above, both the $J_{1/2}$ and the HF model correctly predict the absorption of a circularly polarized laser beam due to a transverse magnetic field, as well as the deflection of such a beam by an inhomogeneous transverse magnetic field [14].

IV. CONCLUSIONS

In spite of several shortcomings, the $J_{1/2}$ model still has its advantages. It is more transparent than the complex HF model, and since it contains only a few equations for the density-matrix components, it can be solved much faster on a computer. Also the wrong time scale of optical pumping effects, which lets the system reach its steady state about an order of magnitude faster, helps to save computing time. The $J_{1/2}$ model is still useful since it describes many effects at least quantitatively correct. For improved qualitative results, however, some adjustments are necessary. (i) The time scale of the results has to be adjusted by a factor of about 5 in order to obtain realistic optical pumping times. (ii) The diffusion constant has to be increased by a factor of about 7 in order to obtain the correct absorption at normal laser intensities. Increasing the density of the vapor as an alternative leads to the desired correction in the steady state, but fails for time-dependent calculations. (iii) The g factors have to be reduced by a factor of 4 to correct the Larmor precession frequency. This is of course related to the time-scale adjustment above. However, the g factors must not be reduced for the simulation of effects that involve the destruction of optical pumping and its resulting change of refractive index, such as the deflection of a circularly polarized beam by the inhomogeneous magnetic field of a current carrying wire [14] or the absorption of a circularly polarized beam by a transverse magnetic field.

For exploring parameters, usually the $J_{1/2}$ model is used in order to save computing time. A calculation with the HF model then delivers the final result for comparison with the experiment.

V. OUTLOOK

A. Two-dimensional sodium vapor

Recent results [28–30] suggest the possibility of holding a two-dimensional gas of sodium atoms near a surface. The binding energy seems to be low enough to disturb the optical properties of the atoms only slightly. The wave equation (6) can be adapted to this two-dimensional case by reducing the thickness of the sodium vapor to zero, resulting in

$$\vec{E}_0(t)_{\mathrm{out}}=\vec{E}_0(t)_{\mathrm{in}}+\frac{i\omega\sigma}{2\varepsilon_0 c}\vec{P}_0(t), \tag{48}$$

where σ is the surface density of the Na atoms and $\vec{E}_0(t)_{\mathrm{in}},\vec{E}_0(t)_{\mathrm{out}}$ are the incoming and outgoing field envelopes, in front of and behind the surface, respectively. The laser beams are assumed to propagate perpendicularly to the surface. The polarization $\vec{P}_0(t)$ is determined by the density-matrix equations as before. While the surface densities σ achieved are still too low to cause observable effects in the steady state, it should be possible to measure quasi-Rabi signals behind such a surface when a fast rising light pulse is turned on as, for example, in [31]. Even though no optical pumping is involved, a simulation (Fig. 5) of such an experiment leads to quite different predictions for the $J_{1/2}$ and the HF model due to the superposition of several Rabi frequencies in the HF model. These Rabi oscillations and their damping constants would reveal information about the sur-

face density σ and the coupling of the atoms to the surface. For high atomic densities, the direct interaction between atoms as well as radiation trapping neglected so far would have to be included in the calculations. Superradiant pulses propagating along the surface and other coherent effects should then be possible.

B. Other alkali-metal atoms

The HF model derived in Sec. II can be adapted to other transitions of sodium or other alkali-metal atoms. In addition to different momenta J and I, the main difference would be the size of the hyperfine splitting energies. As an example, the sodium D_2 transition would require a total of 24×24 equations with this treatment. For cesium, which has nuclear spin $I=7/2$, this number increases to 32×32 (D_1) and 48×48 (D_2) equations for the density-matrix components. Some of these calculations have been done for the steady state, where many of the equations can be neglected. If the dynamic evolution of these systems depends on about the same ratio of necessary equations to total equations as in the presently discussed system, the increase in computing time for a numerical solution would be enormous. A careful study of the circumstances under which some of the elements might be neglected in the dynamic case would be useful, but also difficult because of the increased complexity of these systems.

ACKNOWLEDGMENTS

We wish to thank the Swiss Scientific Computing Center (CSCS) for access to their supercomputing facilities. Also we would like to thank Professor G. Scharf of the Institute for Theoretical Physics, University of Zürich, and Dr. R. Ballagh of Otago University, New Zealand, for help and stimulating discussions. This work was supported by the Schweizer Nationalfonds and the Ernst Hadorn Stiftung.

APPENDIX A: DENSITY-MATRIX EQUATIONS WITH HYPERFINE STRUCTURE

In the simplest case of only one circular polarization ($E_0^-=0$) and no magnetic field, the density-matrix equations reduce to the following set of 34 ordinary differential equations that have to be solved to calculate the polarization (43). One equation can be eliminated using the population conservation relation (17). The equations have been derived using the commercial computer algebra system MATHEMATICA [32]. The following abbreviations apply: $V=dE_0^+/\hbar$ and $\Delta\omega=\omega-\omega_0$, the detuning of the laser from the D_1 transition. Also, as a simplification, we write ${}^{FG}_{lu}\rho^k_q$ instead of ${}^{FG}_{lu}\tilde{\rho}^k_q$ and γ^k_α instead of $\gamma^k_{\alpha\alpha}$. Note that the total hyperfine splittings are $\Delta E_{HF,\alpha}=2\hbar\omega_\alpha$ [Eq. (20)]. The equations for the ll elements are then

$$\dot{{}^{11}_{ll}\rho^0_0}=-\frac{1}{3\sqrt{6}}\mathrm{Im}(V\,{}^{11}_{lu}\rho^1_1)-\sqrt{\frac{5}{54}}\mathrm{Im}(V\,{}^{12}_{lu}\rho^1_1)+\frac{\gamma_{\mathrm{nat}}}{6}({}^{11}_{uu}\rho^0_0+\sqrt{15}\,{}^{22}_{uu}\rho^0_0)-\gamma_{\mathrm{diff}}\left({}^{11}_{ll}\rho^0_0-\frac{\sqrt{3}}{8}\right),$$

$$\dot{{}^{11}_{ll}\rho^1_0}=-\frac{1}{12}\mathrm{Im}[V({}^{11}_{lu}\rho^1_1+{}^{11}_{lu}\rho^2_1-\sqrt{5}\,{}^{12}_{lu}\rho^1_1+3\,{}^{12}_{lu}\rho^2_1)]+\frac{\gamma_{\mathrm{nat}}}{12}[{}^{11}_{uu}\rho^1_0+3\sqrt{5}\,{}^{22}_{uu}\rho^1_0+2\sqrt{5}\,\mathrm{Re}({}^{21}_{uu}\rho^1_0)]-\gamma^1_l\,{}^{11}_{ll}\rho^1_0,$$

$$\dot{{}^{11}_{ll}\rho^2_0}=\frac{1}{60\sqrt{3}}\mathrm{Im}[V(5\,{}^{11}_{lu}\rho^1_1-15\,{}^{11}_{lu}\rho^2_1-\sqrt{5}\,{}^{12}_{lu}\rho^1_1+15\,{}^{12}_{lu}\rho^2_1-12\sqrt{5}\,{}^{12}_{lu}\rho^3_1)]-\frac{\gamma_{\mathrm{nat}}}{12}[{}^{11}_{uu}\rho^2_0-\sqrt{21}\,{}^{22}_{uu}\rho^2_0-6\,\mathrm{Re}({}^{21}_{uu}\rho^2_0)]-\gamma^2_l\,{}^{11}_{ll}\rho^2_0,$$

$$\dot{{}^{21}_{ll}\rho^1_0}=\frac{-i}{120}V^*(5\sqrt{5}\,{}^{11}_{lu}\rho^1_1+\sqrt{5}\,{}^{11}_{lu}\rho^2_1+15\,{}^{12}_{lu}\rho^1_1+3\sqrt{5}\,{}^{12}_{lu}\rho^2_1)^*-(2i\omega_l+\gamma^1_l)\,{}^{21}_{ll}\rho^1_0-\frac{i}{120}V(5\,{}^{21}_{lu}\rho^1_1-3\sqrt{5}\,{}^{21}_{lu}\rho^2_1+15\,{}^{22}_{lu}\rho^1_1-\sqrt{105}\,{}^{22}_{lu}\rho^2_1)$$
$$+\frac{\gamma_{\mathrm{nat}}}{12}(\sqrt{5}\,{}^{11}_{uu}\rho^1_0-3\,{}^{21}_{uu}\rho^1_0+{}^{21}_{uu}\rho^1_0{}^*+3\,{}^{22}_{uu}\rho^1_0),$$

$$\dot{{}^{21}_{ll}\rho^2_0}=\frac{-i}{120\sqrt{3}}V^*(15\,{}^{11}_{lu}\rho^1_1+15\,{}^{11}_{lu}\rho^2_1-3\sqrt{5}\,{}^{12}_{lu}\rho^1_1+25\,{}^{12}_{lu}\rho^2_1+4\sqrt{5}\,{}^{12}_{lu}\rho^3_1)^*-(2i\omega_l+\gamma^2_l)\,{}^{21}_{ll}\rho^2_0$$
$$-\frac{i}{360}V(3\sqrt{15}\,{}^{21}_{lu}\rho^1_1-5\sqrt{3}\,{}^{21}_{lu}\rho^2_1-4\sqrt{15}\,{}^{21}_{lu}\rho^3_1-3\sqrt{15}\,{}^{22}_{lu}\rho^1_1+15\sqrt{7}\,{}^{22}_{lu}\rho^2_1-12\sqrt{10}\,{}^{22}_{lu}\rho^3_1)$$
$$+\frac{\gamma_{\mathrm{nat}}}{12}(3\,{}^{11}_{uu}\rho^2_0-{}^{21}_{uu}\rho^2_0+3\,{}^{21}_{uu}\rho^2_0{}^*+\sqrt{21}\,{}^{22}_{uu}\rho^2_0),$$

$$\dot{{}^{22}_{ll}\rho^0_0}=\frac{1}{3\sqrt{2}}\mathrm{Im}(V\,{}^{21}_{lu}\rho^1_1+V\,{}^{22}_{lu}\rho^1_1)+\frac{\gamma_{\mathrm{nat}}}{6}(\sqrt{15}\,{}^{11}_{uu}\rho^0_0+3\,{}^{22}_{uu}\rho^0_0)-\gamma_{\mathrm{diff}}\left({}^{22}_{ll}\rho^0_0-\frac{\sqrt{5}}{8}\right),$$

$$\dot{{}^{22}_{ll}\rho^1_0}=\frac{1}{60}\mathrm{Im}(15V\,{}^{21}_{lu}\rho^1_1+3\sqrt{5}V\,{}^{21}_{lu}\rho^2_1+5V\,{}^{22}_{lu}\rho^1_1+\sqrt{105}V\,{}^{22}_{lu}\rho^2_1)+\frac{\gamma_{\mathrm{nat}}}{12}[3\sqrt{5}\,{}^{11}_{uu}\rho^1_0+5\,{}^{22}_{uu}\rho^1_0+6\,\mathrm{Re}({}^{21}_{uu}\rho^1_0)]-\gamma^1_l\,{}^{22}_{ll}\rho^1_0,$$

$$\dot{{}^{22}_{ll}\rho^2_0}=\frac{1}{420}\mathrm{Im}(7\sqrt{35}V\,{}^{21}_{lu}\rho^1_1+35\sqrt{7}V\,{}^{21}_{lu}\rho^2_1+4\sqrt{35}V\,{}^{21}_{lu}\rho^3_1-7\sqrt{35}V\,{}^{22}_{lu}\rho^1_1+35\sqrt{3}V\,{}^{22}_{lu}\rho^2_1+4\sqrt{210}V\,{}^{22}_{lu}\rho^3_1)$$
$$+\frac{\gamma_{\mathrm{nat}}}{12}[\sqrt{21}{}^{11}_{uu}\rho^2_0+3\,{}^{22}_{uu}\rho^2_0+2\sqrt{21}\mathrm{Re}({}^{21}_{uu}\rho^2_0)]-\gamma^2_l\,{}^{22}_{ll}\rho^2_0,$$

$$\dot{{}^{21}_{ll}\rho^3_0}=\frac{-i}{30\sqrt{6}}V^*(3\sqrt{5}\,{}^{11}_{lu}\rho^2_1{}^*-\sqrt{5}\,{}^{12}_{lu}\rho^2_1{}^*+10\,{}^{12}_{lu}\rho^3_1{}^*)+(-2i\omega_l-\gamma^3_l){}^{21}_{ll}\rho^3_0$$
$$-\frac{i}{1260}V(7\sqrt{30}\,{}^{21}_{lu}\rho^2_1-35\sqrt{6}\,{}^{21}_{lu}\rho^3_1-3\sqrt{70}\,{}^{22}_{lu}\rho^2_1+105\,{}^{22}_{lu}\rho^3_1-15\sqrt{105}\,{}^{22}_{lu}\rho^4_1)$$
$$+\frac{\gamma_{\mathrm{nat}}}{6}({}^{21}_{uu}\rho^3_0+3\,{}^{21}_{uu}\rho^3_0{}^*+\sqrt{6}\,{}^{22}_{uu}\rho^3_0),$$

$$\dot{{}^{22}_{ll}\rho^3_0}=\mathrm{Im}\left(\frac{V\,{}^{21}_{lu}\rho^2_1}{3\sqrt{5}}+\frac{V\,{}^{21}_{lu}\rho^3_1}{6}-\frac{V\,{}^{22}_{lu}\rho^2_1}{\sqrt{105}}+\frac{V\,{}^{22}_{lu}\rho^3_1}{2\sqrt{6}}+\frac{1}{6}\sqrt{\frac{5}{14}}V\,{}^{22}_{lu}\rho^4_1\right)-\gamma^3_l\,{}^{22}_{ll}\rho^3_0+\sqrt{\frac{2}{3}}\gamma_{\mathrm{nat}}\mathrm{Re}({}^{21}_{uu}\rho^3_0),$$

$$\dot{{}^{22}_{ll}\rho^4_0}=\mathrm{Im}\left(\frac{V\,{}^{21}_{lu}\rho^3_1}{2\sqrt{7}}-\frac{V\,{}^{22}_{lu}\rho^3_1}{2\sqrt{42}}+\frac{1}{6}\sqrt{\frac{5}{2}}V\,{}^{22}_{lu}\rho^4_1\right)-\gamma^4_l\,{}^{22}_{ll}\rho^4_0-\frac{\gamma_{\mathrm{nat}}\,{}^{22}_{uu}\rho^4_0}{3}.$$

For the uu elements we obtain

$$\dot{{}^{11}_{uu}\rho^0_0}=\frac{1}{3\sqrt{6}}\mathrm{Im}(V\,{}^{11}_{lu}\rho^1_1)-\frac{1}{3}\sqrt{\frac{5}{6}}\mathrm{Im}(V\,{}^{21}_{lu}\rho^1_1)-(\gamma_{\mathrm{nat}}+\gamma_{\mathrm{diff}})\,{}^{11}_{uu}\rho^0_0,$$

$$\dot{{}^{11}_{uu}\rho^1_0}=-\frac{1}{12}\mathrm{Im}[V({}^{11}_{lu}\rho^1_1-{}^{11}_{lu}\rho^2_1+\sqrt{5}\,{}^{21}_{lu}\rho^1_1+3\,{}^{21}_{lu}\rho^2_1)]-\gamma^1_u\,{}^{11}_{uu}\rho^1_0,$$

$$\dot{{}^{11}_{uu}\rho^2_0}=-\frac{1}{60\sqrt{3}}\mathrm{Im}[V(5\,{}^{11}_{lu}\rho^1_1+15\,{}^{11}_{lu}\rho^2_1+\sqrt{5}\,{}^{21}_{lu}\rho^1_1+15\,{}^{21}_{lu}\rho^2_1+12\sqrt{5}\,{}^{21}_{lu}\rho^3_1)]-\gamma^2_u\,{}^{11}_{uu}\rho^2_0,$$

$$\dot{{}^{21}_{uu}\rho^1_0}=\frac{i}{120}V(5\sqrt{5}\,{}^{11}_{lu}\rho^1_1-\sqrt{5}\,{}^{11}_{lu}\rho^2_1-15\,{}^{21}_{lu}\rho^1_1+3\sqrt{5}\,{}^{21}_{lu}\rho^2_1)-(2i\omega_u+\gamma^1_u){}^{21}_{uu}\rho^1_0$$
$$-\frac{i}{120}V^*(5\,{}^{12}_{lu}\rho^1_1+3\sqrt{5}\,{}^{12}_{lu}\rho^2_1-15\,{}^{22}_{lu}\rho^1_1-\sqrt{105}\,{}^{22}_{lu}\rho^2_1)^*,$$

$$\dot{{}^{21}_{uu}\rho^2_0}=\frac{-i}{120\sqrt{3}}V(15\,{}^{11}_{lu}\rho^1_1-15\,{}^{11}_{lu}\rho^2_1+3\sqrt{5}\,{}^{21}_{lu}\rho^1_1+25\,{}^{21}_{lu}\rho^2_1-4\sqrt{5}\,{}^{21}_{lu}\rho^3_1)-(2i\omega_u+\gamma^2_u){}^{21}_{uu}\rho^2_0$$
$$+\frac{i}{360}V^*(3\sqrt{15}\,{}^{12}_{lu}\rho^1_1+5\sqrt{3}\,{}^{12}_{lu}\rho^2_1-4\sqrt{15}\,{}^{12}_{lu}\rho^3_1+3\sqrt{15}\,{}^{22}_{lu}\rho^1_1+15\sqrt{7}\,{}^{22}_{lu}\rho^2_1+12\sqrt{10}\,{}^{22}_{lu}\rho^3_1)^*,$$

$$\dot{{}^{22}_{uu}\rho^0_0}=\frac{1}{3\sqrt{2}}\mathrm{Im}(V\,{}^{12}_{lu}\rho^1_1-V\,{}^{22}_{lu}\rho^1_1)-(\gamma_{\mathrm{nat}}+\gamma_{\mathrm{diff}})\,{}^{22}_{uu}\rho^0_0,$$

$$\dot{{}^{22}_{uu}\rho^1_0}=\frac{1}{60}\mathrm{Im}(-15V\,{}^{12}_{lu}\rho^1_1+3\sqrt{5}V\,{}^{12}_{lu}\rho^2_1+5V{}^{22}_{lu}\rho^1_1-\sqrt{105}V\,{}^{22}_{lu}\rho^2_1)-\gamma^1_u\,{}^{22}_{uu}\rho^1_0,$$

$$\dot{{}^{22}_{uu}\rho^2_0}=\frac{1}{420}\mathrm{Im}(7\sqrt{35}V\,{}^{12}_{lu}\rho^1_1-35\sqrt{7}V\,{}^{12}_{lu}\rho^2_1+4\sqrt{35}V\,{}^{12}_{lu}\rho^3_1+7\sqrt{35}V\,{}^{22}_{lu}\rho^1_1+35\sqrt{3}V\,{}^{22}_{lu}\rho^2_1-4\sqrt{210}V\,{}^{22}_{lu}\rho^3_1)-\gamma^2_u\,{}^{22}_{uu}\rho^2_0,$$

$$\dot{{}^{21}_{uu}\rho^3_0}=\frac{-i}{30\sqrt{6}}V(3\sqrt{5}\,{}^{11}_{lu}\rho^2_1+\sqrt{5}\,{}^{21}_{lu}\rho^2_1+10\,{}^{21}_{lu}\rho^3_1)+(-2i\omega_u-\gamma^3_u){}^{21}_{uu}\rho^3_0$$
$$+\frac{i}{1260}V^*(7\sqrt{30}\,{}^{12}_{lu}\rho^2_1+35\sqrt{6}\,{}^{12}_{lu}\rho^3_1+3\sqrt{70}\,{}^{22}_{lu}\rho^2_1+105\,{}^{22}_{lu}\rho^3_1+15\sqrt{105}\,{}^{22}_{lu}\rho^4_1)^*,$$

$$\dot{{}^{22}_{uu}\rho^3_0}=\mathrm{Im}\left(\frac{V\,{}^{12}_{lu}\rho^2_1}{3\sqrt{5}}-\frac{V\,{}^{12}_{lu}\rho^3_1}{6}+\frac{V\,{}^{22}_{lu}\rho^2_1}{\sqrt{105}}+\frac{V\,{}^{22}_{lu}\rho^3_1}{2\sqrt{6}}-\frac{\sqrt{5}V\,{}^{22}_{lu}\rho^4_1}{6\sqrt{14}}\right)-\gamma^3_u\,{}^{22}_{uu}\rho^3_0,$$

$$\dot{{}^{22}_{uu}\rho^4_0}=\mathrm{Im}\left(\frac{V\,{}^{12}_{lu}\rho^3_1}{2\sqrt{7}}+\frac{V\,{}^{22}_{lu}\rho^3_1}{2\sqrt{42}}+\frac{\sqrt{5}V\,{}^{22}_{lu}\rho^4_1}{6\sqrt{2}}\right)-\gamma^4_u\,{}^{22}_{uu}\rho^4_0,$$

and finally the lu elements are

$$\dot{{}^{11}_{lu}\rho^1_1}=[i(-\Delta\omega+\omega_l-\omega_u)-\gamma^1_{lu}]{}^{11}_{lu}\rho^1_1+\frac{i}{72}V^*(2\sqrt{6}\,{}^{11}_{ll}\rho^0_0+3\,{}^{11}_{ll}\rho^1_0-\sqrt{3}\,{}^{11}_{ll}\rho^2_0-2\sqrt{6}\,{}^{11}_{uu}\rho^0_0+3\,{}^{11}_{uu}\rho^1_0+\sqrt{3}\,{}^{11}_{uu}\rho^2_0+3\sqrt{5}\,{}^{21}_{ll}\rho^1_0{}^*$$
$$+3\sqrt{3}\,{}^{21}_{ll}\rho^2_0{}^*+3\sqrt{5}\,{}^{21}_{uu}\rho^1_0-3\sqrt{3}\,{}^{21}_{uu}\rho^2_0),$$

$$\dot{{}^{21}_{lu}\rho^1_1}=[i(-\Delta\omega-\omega_l-\omega_u)-\gamma^1_{lu}]{}^{21}_{lu}\rho^1_1+\frac{i}{360}V^*(10\sqrt{30}\,{}^{11}_{uu}\rho^0_0+15\sqrt{5}\,{}^{11}_{uu}\rho^1_0+\sqrt{15}\,{}^{11}_{uu}\rho^2_0-15\,{}^{21}_{ll}\rho^1_0-3\sqrt{15}\,{}^{21}_{ll}\rho^2_0-45\,{}^{21}_{uu}\rho^1_0$$
$$-3\sqrt{15}\,{}^{21}_{uu}\rho^2_0-30\sqrt{2}\,{}^{22}_{ll}\rho^0_0-45\,{}^{22}_{ll}\rho^1_0-3\sqrt{35}\,{}^{22}_{ll}\rho^2_0),$$

$$\dot{{}^{12}_{lu}\rho^1_1}=[i(-\Delta\omega+\omega_l+\omega_u)-\gamma^1_{lu}]{}^{12}_{lu}\rho^1_1+\frac{i}{360}V^*(10\sqrt{30}\,{}^{11}_{ll}\rho^0_0-15\sqrt{5}\,{}^{11}_{ll}\rho^1_0+\sqrt{15}\,{}^{11}_{ll}\rho^2_0+45\,{}^{21}_{ll}\rho^1_0{}^*-3\sqrt{15}\,{}^{21}_{ll}\rho^2_0{}^*+15\,{}^{21}_{uu}\rho^1_0{}^*$$
$$-3\sqrt{15}\,{}^{21}_{uu}\rho^2_0{}^*-30\sqrt{2}\,{}^{22}_{uu}\rho^0_0+45\,{}^{22}_{uu}\rho^1_0-3\sqrt{35}\,{}^{22}_{uu}\rho^2_0),$$

$$\dot{{}^{22}_{lu}\rho^1_1}=[i(-\Delta\omega-\omega_l+\omega_u)-\gamma^1_{lu}]{}^{22}_{lu}\rho^1_1-\frac{i}{120}V^*(15\,{}^{21}_{ll}\rho^1_0-\sqrt{15}\,{}^{21}_{ll}\rho^2_0+15\,{}^{21}_{uu}\rho^1_0{}^*+\sqrt{15}\,{}^{21}_{uu}\rho^2_0{}^*+10\sqrt{2}\,{}^{22}_{ll}\rho^0_0+5\,{}^{22}_{ll}\rho^1_0-\sqrt{35}\,{}^{22}_{ll}\rho^2_0$$
$$-10\sqrt{2}\,{}^{22}_{uu}\rho^0_0+5\,{}^{22}_{uu}\rho^1_0+\sqrt{35}\,{}^{22}_{uu}\rho^2_0),$$

$$\dot{{}^{11}_{lu}\rho^2_1}=[i(-\Delta\omega+\omega_l-\omega_u)-\gamma^2_{lu}]{}^{11}_{lu}\rho^2_1+\frac{i}{120}V^*(5\,{}^{11}_{ll}\rho^1_0+5\sqrt{3}\,{}^{11}_{ll}\rho^2_0-5\,{}^{11}_{uu}\rho^1_0+5\sqrt{3}\,{}^{11}_{uu}\rho^2_0+\sqrt{5}\,{}^{21}_{ll}\rho^1_0{}^*+5\sqrt{3}\,{}^{21}_{ll}\rho^2_0{}^*+2\sqrt{30}\,{}^{21}_{ll}\rho^3_0{}^*$$
$$-\sqrt{5}\,{}^{21}_{uu}\rho^1_0+5\sqrt{3}\,{}^{21}_{uu}\rho^2_0-2\sqrt{30}\,{}^{21}_{uu}\rho^3_0),$$

$$\dot{{}^{12}_{lu}\rho^2_1}=[i(-\Delta\omega+\omega_l+\omega_u)-\gamma^2_{lu}]{}^{12}_{lu}\rho^2_1+\frac{i}{360}V^*(45\,{}^{11}_{ll}\rho^1_0-15\sqrt{3}\,{}^{11}_{ll}\rho^2_0+9\sqrt{5}\,{}^{21}_{ll}\rho^1_0{}^*+25\sqrt{3}\,{}^{21}_{ll}\rho^2_0{}^*-2\sqrt{30}\,{}^{21}_{ll}\rho^3_0{}^*+9\sqrt{5}\,{}^{21}_{uu}\rho^1_0{}^*$$
$$-5\sqrt{3}\,{}^{21}_{uu}\rho^2_0{}^*-2\sqrt{30}\,{}^{21}_{uu}\rho^3_0{}^*-9\sqrt{5}\,{}^{22}_{uu}\rho^1_0+15\sqrt{7}\,{}^{22}_{uu}\rho^2_0-12\sqrt{5}\,{}^{22}_{uu}\rho^3_0),$$

$$\dot{{}^{12}_{lu}\rho^3_1}=[i(-\Delta\omega+\omega_l+\omega_u)-\gamma^3_{lu}]{}^{12}_{lu}\rho^3_1+\frac{i}{1260}V^*(42\sqrt{15}\,{}^{11}_{ll}\rho^2_0+14\sqrt{15}\,{}^{21}_{ll}\rho^2_0{}^*+70\sqrt{6}\,{}^{21}_{ll}\rho^3_0{}^*+14\sqrt{15}\,{}^{21}_{uu}\rho^2_0{}^*-35\sqrt{6}\,{}^{21}_{uu}\rho^3_0{}^*$$
$$-6\sqrt{35}\,{}^{22}_{uu}\rho^2_0+105\,{}^{22}_{uu}\rho^3_0-45\sqrt{7}\,{}^{22}_{uu}\rho^4_0),$$

$$\dot{{}^{21}_{lu}\rho^2_1}=[i(-\Delta\omega-\omega_l-\omega_u)-\gamma^2_{lu}]{}^{21}_{lu}\rho^2_1+\frac{i}{360}V^*(45\,{}^{11}_{uu}\rho^1_0+15\sqrt{3}\,{}^{11}_{uu}\rho^2_0+5\sqrt{3}\,{}^{21}_{ll}\rho^2_0-2\sqrt{30}\,{}^{21}_{ll}\rho^3_0-25\sqrt{3}\,{}^{21}_{uu}\rho^2_0-2\sqrt{30}\,{}^{21}_{uu}\rho^3_0$$
$$+9\sqrt{5}({}^{21}_{ll}\rho^1_0+{}^{21}_{uu}\rho^1_0-{}^{22}_{ll}\rho^1_0)-15\sqrt{7}\,{}^{22}_{ll}\rho^2_0-12\sqrt{5}\,{}^{22}_{ll}\rho^3_0),$$

$$\dot{{}^{21}_{lu}\rho^3_1}=[i(-\Delta\omega-\omega_l-\omega_u)-\gamma^3_{lu}]{}^{21}_{lu}\rho^3_1+\frac{i}{1260}V^*(42\sqrt{15}\,{}^{11}_{uu}\rho^2_0+14\sqrt{15}\,{}^{21}_{ll}\rho^2_0+35\sqrt{6}\,{}^{21}_{ll}\rho^3_0+14\sqrt{15}\,{}^{21}_{uu}\rho^2_0-70\sqrt{6}\,{}^{21}_{uu}\rho^3_0$$
$$-6\sqrt{35}\,{}^{22}_{ll}\rho^2_0-105\,{}^{22}_{ll}\rho^3_0-45\sqrt{7}\,{}^{22}_{ll}\rho^4_0),$$

$$
{}^{22}_{lu}\dot{\rho}^{2}_{1}=[i(-\Delta\omega-\omega_l+\omega_u)-\gamma^{2}_{lu}]{}^{22}_{lu}\rho^{2}_{1}-\frac{i}{840}V^{*}[35\sqrt{7}\ {}^{21}_{ll}\rho^{2}_{0}-2\sqrt{70}\ {}^{21}_{ll}\rho^{3}_{0}+35\sqrt{7}\ {}^{21}_{uu}\rho^{2}_{0}{}^{*}+2\sqrt{70}\ {}^{21}_{uu}\rho^{3}_{0}{}^{*}+35\sqrt{3}\ {}^{22}_{ll}\rho^{2}_{0}
$$

$$
-4\sqrt{105}\ {}^{22}_{ll}\rho^{3}_{0}+7\sqrt{105}(-{}^{21}_{ll}\rho^{1}_{0}+{}^{21}_{uu}\rho^{1}_{0}{}^{*}+{}^{22}_{ll}\rho^{1}_{0}-{}^{22}_{uu}\rho^{1}_{0})+35\sqrt{3}\ {}^{22}_{uu}\rho^{2}_{0}+4\sqrt{105}\ {}^{22}_{uu}\rho^{3}_{0}],
$$

$$
{}^{22}_{lu}\dot{\rho}^{3}_{1}=\Big[i(-\Delta\omega-\omega_l+\omega_u-\gamma^{3}_{lu}]{}^{22}_{lu}\rho^{3}_{1}-\frac{i}{840}V^{*}[28\sqrt{10}(-{}^{21}_{ll}\rho^{2}_{0}+{}^{21}_{uu}\rho^{2}_{0}{}^{*})+70({}^{21}_{ll}\rho^{3}_{0}+{}^{21}_{uu}\rho^{3}_{0}{}^{*})+4\sqrt{210}({}^{22}_{ll}\rho^{2}_{0}-{}^{22}_{uu}\rho^{2}_{0})+35\sqrt{6}({}^{22}_{ll}\rho^{3}_{0}
$$

$$
+{}^{22}_{uu}\rho^{3}_{0})-5\sqrt{42}({}^{22}_{ll}\rho^{4}_{0}-{}^{22}_{uu}\rho^{4}_{0})],
$$

$$
{}^{22}_{lu}\dot{\rho}^{4}_{1}=[i(-\Delta\omega-\omega_l+\omega_u)-\gamma^{4}_{lu}]{}^{22}_{lu}\rho^{4}_{1}-\frac{i}{168}\sqrt{5}V^{*}[2\sqrt{21}(-{}^{21}_{ll}\rho^{3}_{0}+{}^{21}_{uu}\rho^{3}_{0}{}^{*})+\sqrt{14}({}^{22}_{ll}\rho^{3}_{0}-{}^{22}_{uu}\rho^{3}_{0})+7\sqrt{2}({}^{22}_{ll}\rho^{4}_{0}+{}^{22}_{uu}\rho^{4}_{0})].
$$

APPENDIX B: DENSITY-MATRIX EQUATIONS FOR THE $J=1/2\leftrightarrow J=1/2$ APPROXIMATION

For completeness, we include here the time-dependent $J=1/2\leftrightarrow J=1/2$ density-matrix equations. Again, for the simplest case of $\vec{B}=0$ and $E_0^-=0$, and writing ${}_{lu}\rho^{k}_{q}$ instead of ${}_{lu}\tilde{\rho}^{k}_{q}$, one obtains

$$
{}_{ll}\dot{\rho}^{0}_{0}=\gamma_{\rm nat}\left(\frac{1}{\sqrt{2}}-{}_{ll}\rho^{0}_{0}\right)+\mathrm{Im}(F\,{}_{lu}\rho^{1}_{1}),
$$

$$
{}_{ll}\dot{\rho}^{1}_{0}=-\gamma_l\ {}_{ll}\rho^{1}_{0}-\frac{\gamma_{\rm nat}}{3}{}_{uu}\rho^{1}_{0}+\mathrm{Im}(F\,{}_{lu}\rho^{1}_{1}),
$$

$$
{}_{uu}\dot{\rho}^{1}_{0}=-\gamma_u\ {}_{uu}\rho^{1}_{0}+\mathrm{Im}(F\,{}_{lu}\rho^{1}_{1}),
$$

$$
{}_{lu}\dot{\rho}^{1}_{1}=-(\gamma_{lu}+i\Delta\omega)\,{}_{lu}\rho^{1}_{1}+\frac{iF^{*}}{2}\left(\frac{1}{\sqrt{2}}-2\ {}_{ll}\rho^{0}_{0}-{}_{uu}\rho^{1}_{0}-{}_{ll}\rho^{1}_{0}\right).
$$

Here the electric field is $F=\sqrt{2}d_{1/2}E_0^+$, with E_0^+ as defined in Eqs. (1) and (8). The macroscopic polarization component P_0^+ is related to the equations by

$$
P_0^+=\frac{2nd_{1/2}}{\sqrt{3}}{}_{lu}\rho^{1}_{1}{}^{*}, \tag{B1}
$$

where $d_{1/2}$ is the reduced matrix element of the $J=1/2\leftrightarrow J=1/2$ approximation

$$
d_{1/2}=\sqrt{\frac{6\gamma_{\rm nat}\pi\hbar c^{3}\varepsilon_0}{\omega_0^{3}}}=\frac{2}{\sqrt{3}}d. \tag{B2}
$$

[1] R. P. Feynman, F. L. Vernon, and R. W. Helwarth, J. Appl. Phys. **28**, 49 (1957).
[2] B. R. Mollow, Phys. Rev. A **12**, 1919 (1975).
[3] E. T. Jaynes and F. W. Cummings, Proc. IEEE **51**, 89 (1963).
[4] S. Dangel *et al.*, J. Opt. Soc. Am. B **12**, 681 (1995).
[5] M. Ducloy, Phys. Rev. A **8**, 1844 (1973).
[6] A. Omont, Prog. Quantum Electron. **5**, 69 (1977).
[7] U. Fano, Rev. Mod. Phys. **29**, 74 (1957).
[8] A. W. McCord and R. J. Ballagh, J. Opt. Soc. Am. B **7**, 73 (1990).
[9] W. Happer, Rev. Mod. Phys. **44**, 169 (1972).
[10] R. Holzner, P. Eschle, A. W. McCord, and D. M. Warrington, Phys. Rev. Lett. **69**, 2192 (1992).
[11] B. Röhricht *et al.*, Opt. Commun. **118**, 601 (1995).
[12] B. Röhricht *et al.*, Phys. Rev. A **50**, 2434 (1994).
[13] R. J. Ballagh and A. W. McCord, in *International Conference on Quantum Electronics Technical Digest Series 1992* (IQEC, Vienna, 1992), Vol. 9, pp. 520–522.
[14] R. Holzner *et al.*, Phys. Rev. Lett. **78**, 3451 (1997).
[15] D. Suter, Phys. Rev. A **46**, 344 (1992).
[16] G. M. Meyer *et al.*, Quantum Opt. **6**, 231 (1994).
[17] D. E. Nikonov *et al.*, Quantum Opt. **6**, 245 (1994).
[18] G. G. Padmabandu *et al.*, Quantum Opt. **6**, 261 (1994).
[19] S. Dangel and R. Holzner, J. Opt. Soc. Am. B (to be published).
[20] A. R. Edmonds, *Angular Momentum in Quantum Mechanics* (Princeton University Press, Princeton, 1957).
[21] R. Loudon, *The Quantum Theory of Light* (Clarendon, Oxford, 1984).
[22] L. C. Balling, Adv. Quantum Electron. **3**, 1 (1975).
[23] L. Allen and J. H. Eberly, *Optical Resonance and Two-Level Atoms* (Wiley, New York, 1975).

[24] M. Ducloy and M. Dumont, J. Phys. (France) **31**, 419 (1970).
[25] J. A. Vallés and J. M. Alvarez, Phys. Rev. A **50**, 2490 (1994).
[26] D. G. McCartan and J. M. Farr, J. Phys. B **9**, 985 (1976).
[27] E. S. Fry *et al.*, Phys. Rev. Lett. **70**, 3235 (1993).
[28] F. Balzer and H. Rubahn, J. Electron Spectrosc. Relat. Phenom. **64/65**, 321 (1993).
[29] F. Balzer, K. Bammel, and H. Rubahn, J. Chem. Phys. **98**, 7625 (1993).
[30] S. Dangel, Y. Bonetti, and R. Holzner, in *Proceedings of Conference on Atom Optics and Interferometry Digest 1996* (Australian National University, Canberra, 1996), p. PTh16.
[31] P. M. Farrell, W. R. MacGillivray, and M. C. Standage, Phys. Lett. **107A**, 263 (1985).
[32] S. Wolfram, *Mathematica: A System for Doing Mathematics by Computer* (Addison-Wesley, Redwood City, CA, 1991).